VCST Internal Memo

Title: Estimate of the Uncertainty in the JPSS-1 VIIRS Response Versus Scan Measurements
Memo Number: 2015_009
Revision: 01
Date: June 1, 2016
Author: Jeff McIntire
To: Xiaoxiong Xiong and James Butler
Cc: Hassan Oudrari, Kwo-Fu (Vincent) Chiang, Jon Fulbright and Aisheng Wu

---

References

[1] VCST_TECH_MEMO_2014_018, 'Analysis of FP-10 Part 2 Thermal Band Response Versus Scan Angle Determination,' Jeff McIntire, August 15, 2014.
[2] VCST_TECH_REPORT_14_027, 'VIIRS Response Versus Scan for the Reflective Solar Bands,' Tom Schwarting, Shihyan Lee, and Jeff McIntire, April 16, 2014.
[3] An Introduction to Error Analysis, John R. Taylor, University Science Books, 1997.
[4] VCST_TECH_MEMO_2015_018, 'Estimate of the Radiometric Uncertainty for the JPSS-1 VIIRS Thermal Bands,' Jeff McIntire, November 16, 2015.
[7] 'Response Versus Scan angle Test FP-10 Test Procedure – VIIRS,' TP154640-2221.

1. Introduction

VIIRS response versus scan (RVS) angle measurements were made during FP-10 testing (part 1 for reflective bands and part 2 for thermal bands) [1-2]. The uncertainty analysis in these works estimated the uncertainty as the average fitting residual. However, the uncertainty of the RVS should be scan angle dependent, with zero uncertainty at the normalization point and increasing uncertainty at lower HAM AOI. In this work, we seek to propagate the uncertainties in the test to the final RVS for both the reflective and thermal bands, using a standard formulation [3]. It is important to estimate the uncertainty of these measurements for science team evaluations of the down stream products. The data used in this work is listed in Tables 1 and 2.

2. Error Propagation

For the purposes of this work, we follow the standard propagation of error for a function y of variables x_i is described by [3]

$$u^2(y) = \sum_{i=1}^{N}\left(\frac{\partial y}{\partial x_i}\right)^2 u^2(x_i) + 2\sum_{i=1}^{N-1}\sum_{j=i+1}^{N}\left(\frac{\partial y}{\partial x_i}\right)\left(\frac{\partial y}{\partial x_j}\right)u(x_i, x_j). \tag{1}$$

Here $u(x_i)$ is the uncertainty of the variable x_i that goes into the calculation of the y and $u(x_i,x_j)$ is the covariance between x_i and x_j.

The measured RVS was defined in [1] for the thermal bands and is a function of

$$RVS_{meas} = f\left(L_{LABB}, L_{OBCBB}, L_{RTA}, L_{CAV}, L_{SH}, L_{HAM}, F_{SH}, F_{CAV}, F_{RTA}, \varepsilon_{BB}, \rho_{RTA}, dn_{LABB}, dn_{OBCBB}\right). \tag{2}$$

The partial derivatives for each variable are listed in Appendix A. The measured uncertainties are then propagated into the fitting of a quadratic polynomial in HAM AOI. For the reflective bands, the measured RVS is only dependent on the dn uncertainty (which includes source drift). The final RVS uncertainty is then a function of

$$RVS = f\left(a_0, a_1, a_2, AOI, RVS_{meas}\right). \tag{3}$$

The partial derivatives for each variable are listed in Appendix B.

In general, the covariance terms were not directly calculated (the exceptions are the covariance terms between the fitting coefficients); a direct calculation of these terms is beyond the scope of this work. However, an upper bound on the covariance terms is determined through use of the Schwarz inequality [1], or

$$\left|u\left(x_i, x_j\right)\right| \le u\left(x_i\right)u\left(x_j\right). \tag{4}$$

Note that when the Schwarz inequality is used in conjunction with Eq. (1), the absolute value of the partial derivatives in the covariance terms are used. Results will be presented with the covariance terms determined using the Schwarz inequality as a worst case estimate. Note that covariance terms are only included in the worst case estimate if the sources of uncertainty are considered interdependent.

3. Individual Thermal Band Error Sources

In this section we describe the individual uncertainty contributors to the thermal band RVS. Some of the descriptions are drawn from [4].

3.1 Radiances

The radiance uncertainty for each of the radiances that factor into the present calculation (L_{LABB}, L_{SVS}, L_{OBCBB}, L_{HAM}, L_{RTA}, L_{SH}, and L_{CAV}) is only the statistical uncertainty. Each of these radiances was converted from a temperature reading provided by one or more thermistors once per scan using the Planck equation, integrated over the spectral response of the instrument. In the cases where more than one thermistor was used, the average was employed in the Planck equation. The statistical uncertainties were the standard deviation of the radiances determined within one collect (or over 100 scans).

3.2LABB, OBCBB, and SV Response

The uncertainty in the response was the RSS of the random and bias errors for the background subtracted digital response. The precision error was the standard deviation of the mean over all analyzed samples and scans. For the purposes of this work, the random error for the LABB, OBCBB SV response was the standard deviation of the mean over the samples used per scan and all scans. All of the known biases were common to all sectors and are therefore removed in the background subtraction [4]. The exception is the M13 bias between auto and fixed gain modes; as this bias is not currently understood and does not affect the results, it was not included in this analysis.

3.3 Other Uncertainties

A number of uncertainty contributors were not considered in the above sections because the RVS is a normalized quantity. As such any term which is considered a bias to all measurements for a given band and detector will not contribute. Error contributors for the thermal bands which did not enter into this calculation include the temperature and spectral biases on the radiance uncertainty, the BB emissivity, and the reflectance of the RTA [4].

4. Individual Reflective Band Error Sources

The individual uncertainty contributors to the reflective band RVS are the uncertainties in the response.

There is a source drift correction used in the RVS calculation that must also be included in the response uncertainty [2]. Here the response uncertainty is modeled as the RSS of the statistical uncertainty in the response and the uncertainty introduced by the source drift correction. The random error for the response was the standard deviation of the mean over the samples used per scan and all scans. The drift correction fit a quadratic polynomial in time to the repeated measurements at -8 degrees scan angle. The drift correction uncertainty is then taken to be the standard deviation of the mean of the corrected -8 degree repeated measurements.

5. Fitting Coefficients

The vertical least-squares fitting algorithm used determined the vertical deviations of the set of data points from the fit, or

$$R^2 = \sum_i \frac{1}{u^2(RVS_i)} \left(RVS_i - c_0 - c_1 dn_i - c_2 dn_i^2\right)^2 . \tag{7}$$

The minimum of the vertical deviations was computed by setting the partial derivatives with respect to coefficients equal to zero, or

$$\frac{\partial R^2}{\partial c_i} = 0 . \tag{8}$$

This led to the following matrix equation:

$$\begin{bmatrix} c_0 \\ c_1 \\ c_2 \end{bmatrix} = \begin{bmatrix} \sum \frac{1}{u^2} & \sum \frac{dn}{u^2} & \sum \frac{dn^2}{u^2} \\ \sum \frac{dn}{u^2} & \sum \frac{dn^2}{u^2} & \sum \frac{dn^3}{u^2} \\ \sum \frac{dn^2}{u^2} & \sum \frac{dn^3}{u^2} & \sum \frac{dn^4}{u^2} \end{bmatrix}^{-1} \begin{bmatrix} \sum \frac{\Delta L}{u^2} \\ \sum \frac{dn \Delta L}{u^2} \\ \sum \frac{dn^2 \Delta L}{u^2} \end{bmatrix}, \tag{9}$$

and we define

$$A = \begin{bmatrix} \sum \frac{1}{u^2} & \sum \frac{dn}{u^2} & \sum \frac{dn^2}{u^2} \\ \sum \frac{dn}{u^2} & \sum \frac{dn^2}{u^2} & \sum \frac{dn^3}{u^2} \\ \sum \frac{dn^2}{u^2} & \sum \frac{dn^3}{u^2} & \sum \frac{dn^4}{u^2} \end{bmatrix}^{-1} . \tag{10}$$

The solution to this matrix equation determined the RVS fitting coefficients. This algorithm also produced 1-sigma uncertainties and covariance terms, which are defined by the following:

$$u(c_i) = \sqrt{A(i,i)} , \tag{11}$$

$$u(c_i, c_j) = A(i, j). \tag{12}$$

The uncertainties in RVS were estimated using Eq. (1) and the partial derivatives in Appendix A for the thermal bands. The individual contributors were listed in the preceding subsections. The uncertainties in RVS were estimated using Eq. (1) and the response uncertainty for the reflective bands.

6. Total RVS Uncertainty

The RVS uncertainty was propagated into the fitting following sections 3, 4, and 5, then the derived uncertainty in the coefficients was propagated to the uncertainty the final RVS. The final RVS uncertainty also depends on the HAM AOI; the uncertainty carried on AOI was equivalent to 3 unaggregated pixels. This uncertainty is scan angle dependent and was propagated through the scan angle to HAM AOI conversion. The final RVS uncertainty was modeled at HAM AOI of 28.7, 30, 35, 40, 45, 50, 55, 60, and 62 degrees.

7. Results

7.1 Reflective Band RVS Uncertainty

The final RVS uncertainty for all reflective bands is shown in Figure 1 (detector 9, HAM side A). Note that the uncertainty is at a minimum near 60.2 degrees AOI, which is the normalization point. It is not exactly zero in this work because the Schwarz inequality was used and this provides an upper bound on the uncertainty. As expected, the uncertainty increases as one moves away from the normalization point and is worst at the HAM minimum of about 28.7 degrees. Here the maximum uncertainties range from about 0.04 % for M10 to 0.21 % for M6. This is still below the target uncertainty of 0.3 % allocated to the RVS by the sensor vendor as part of their total uncertainty roll up [5]. The band average uncertainties based on the original method are listed in Table 3 [2], excluding outliers; for comparison, the average uncertainty based on the above method (over all detector, excluding outliers, and AOI) are also listed in Table 3. The present estimate of the uncertainty is in general larger than the earlier estimate based on the average fitting residual. The exception is M9, where the present method does not capture the added uncertainty due to water vapor absorption. The larger error in the current method is largely derived from the addition of the drift correction uncertainty. For all bands the largest contributions to the uncertainty are the a_1 and a_2 terms. Figures 2 – 15 show the error bars from [2] and for this work for each reflective band (detector 9, HAM side A). Note again that the present uncertainties are largest at low HAM AOI and are negligible at the normalization point (the SD HAM AOI).

7.2 Thermal Band RVS Uncertainty

The final RVS uncertainty for the thermal bands is shown in Figure 16 (detector 9, HAM side A). Again note that the uncertainty is at a minimum near 60.2 degrees AOI, where the RVS is normalized, and that the uncertainty is not exactly zero due to the Schwarz identity providing an upper bound. As with the reflective bands, the uncertainty increases as the AOI decreases (moving away from the normalization point) and is highest at the HAM minimum. The worst case uncertainties range from 0.09 % for M15 to 0.29 % for I5. Both I4 and I5 show uncertainties for some AOI which are above the 0.2 % target value; all other bands are below their respective target values (0.2 % for M12, M13, M15, and M16 and 0.6 % for M14) [5]. The larger uncertified in the I bands are driven by the BB dn uncertainty contributor; these bands are known to have higher noise (on the order of 3 times larger than the thermal M bands). The band average uncertainties based on the original method are listed in Table 4 [1], along with the average uncertainties based on the above method (over all detectors, excluding outliers, and AOI). The present estimate is larger for bands I4, I5, M12, and M13, while it is smaller for the remaining long wave bands M14 – M16. For all bands the largest contributions to the uncertainty are the a_1 and a_2 terms. Figures 17 – 24 show the error bars from [1] and for this work for each thermal band (detector 9, HAM side A). Note again that the present uncertainties are largest at low HAM AOI and are negligible at the normalization point (the SD HAM AOI).

8. Summary

Uncertainty estimates for the reflective and thermal band RVS were determined by propagating the error estimates from the individual uncertainty sources. The following is a list of findings:

- Total estimated uncertainties in the reflective and thermal bands are maximum at the minimum HAM AOI (about 28.7 degrees) and minimum at the normalization point (about 60.2 degrees).
- Reflective band maximum uncertainties range from about 0.04 % for M10 to 0.21 % for M6. The average over all scan angles is slightly larger than earlier estimates based on the fitting residual. The largest contributor is the repeatability of the measurements.
- Thermal band maximum uncertainties range from 0.09 % for M15 to 0.29 % for I5. The average over all scan angles is larger than earlier estimates based on the fitting residual for the I bands as well as M12 and M13, but smaller for bands M14 – M16. The largest contributor is the uncertainty in the BB dn.

Appendix A

The following are the partial derivatives of the measured thermal band RVS with respect to the various contributors:

$$\frac{\partial RVS_{LABB}}{\partial L_{LABB}} = \frac{RVS_{LABB}}{L_{LABB} - \frac{1}{\rho_{RTA}}\left[L_{HAM} - (1-\rho_{RTA})L_{RTA}\right]}$$

$$\frac{\partial RVS_{LABB}}{\partial L_{SV}} = \frac{RVS_{SV}\left(1 - \frac{dn_{LABB}}{dn_{BB}}\right)}{L_{LABB} - \frac{1}{\rho_{RTA}}\left[L_{HAM} - (1-\rho_{RTA})L_{RTA}\right]}$$

$$\frac{\partial RVS_{LABB}}{\partial L_{RTA}} = \frac{\frac{dn_{LABB}}{dn_{BB}}\left[(1-\varepsilon_{BB})F_{RTA} + (1-RVS_{SV})\frac{(1-\rho_{RTA})}{\rho_{RTA}}\right] + (RVS_{SV} - RVS_{LABB})\frac{(1-\rho_{RTA})}{\rho_{RTA}}}{L_{LABB} - \frac{1}{\rho_{RTA}}\left[L_{HAM} - (1-\rho_{RTA})L_{RTA}\right]}$$

$$\frac{\partial RVS_{LABB}}{\partial L_{BB}} = \frac{\frac{dn_{LABB}}{dn_{BB}}\varepsilon_{BB}}{L_{LABB} - \frac{1}{\rho_{RTA}}\left[L_{HAM} - (1-\rho_{RTA})L_{RTA}\right]}$$

$$\frac{\partial RVS_{LABB}}{\partial L_{SH}} = \frac{\frac{dn_{LABB}}{dn_{BB}}(1-\varepsilon_{BB})F_{SH}}{L_{LABB} - \frac{1}{\rho_{RTA}}\left[L_{HAM} - (1-\rho_{RTA})L_{RTA}\right]}$$

$$\frac{\partial RVS_{LABB}}{\partial L_{CAV}} = \frac{\frac{dn_{LABB}}{dn_{BB}}(1-\varepsilon_{BB})F_{CAV}}{L_{LABB} - \frac{1}{\rho_{RTA}}\left[L_{HAM} - (1-\rho_{RTA})L_{RTA}\right]}$$

$$\frac{\partial RVS_{LABB}}{\partial L_{HAM}} = \frac{RVS_{LABB}\frac{1}{\rho_{RTA}} - RVS_{SV}\frac{1}{\rho_{RTA}} - \frac{dn_{LABB}}{dn_{BB}}(1-RVS_{SV})\frac{1}{\rho_{RTA}}}{L_{LABB} - \frac{1}{\rho_{RTA}}\left[L_{HAM} - (1-\rho_{RTA})L_{RTA}\right]}$$

$$\frac{\partial RVS_{LABB}}{\partial dn_{LABB}}=\frac{\frac{1}{dn_{OBCBB}}\left\{\varepsilon_{BB}L_{BB}+(1-\varepsilon_{BB})(F_{SH}L_{SH}+F_{CAV}L_{CAV}+F_{RTA}L_{RTA})-RVS_{SV}L_{SV}-(1-RVS_{SV})\frac{1}{\rho_{RTA}}\left[L_{HAM}-(1-\rho_{RTA})L_{RTA}\right]\right\}}{L_{LABB}-\frac{1}{\rho_{RTA}}\left[L_{HAM}-(1-\rho_{RTA})L_{RTA}\right]}$$

$$\frac{\partial RVS_{LABB}}{\partial dn_{BB}}=-\frac{\frac{dn_{LABB}}{dn_{BB}^2}\left\{\varepsilon_{BB}L_{BB}+(1-\varepsilon_{BB})(F_{SH}L_{SH}+F_{CAV}L_{CAV}+F_{RTA}L_{RTA})-RVS_{SV}L_{SV}-(1-RVS_{SV})\frac{1}{\rho_{RTA}}\left[L_{HAM}-(1-\rho_{RTA})L_{RTA}\right]\right\}}{L_{LABB}-\frac{1}{\rho_{RTA}}\left[L_{HAM}-(1-\rho_{RTA})L_{RTA}\right]}$$

Appendix B

The following are the partial derivatives of the RVS with respect to the various contributors:

$$\frac{\partial RVS}{\partial a_0}=\frac{\left[a_1(AOI_{SD}-AOI)+a_2(AOI_{SD}^2-AOI^2)\right]}{(a_0+a_1AOI_{SD}+a_2AOI_{SD}^2)^2}$$

$$\frac{\partial RVS}{\partial a_1}=\frac{\left[a_0(AOI-AOI_{SD})+a_2(AOIAOI_{SD}^2-AOI^2AOI_{SD})\right]}{(a_0+a_1AOI_{SD}+a_2AOI_{SD}^2)^2}$$

$$\frac{\partial RVS}{\partial a_2}=\frac{\left[a_0(AOI^2-AOI_{SD}^2)+a_1(AOI^2AOI_{SD}-AOIAOI_{SD}^2)\right]}{(a_0+a_1AOI_{SD}+a_2AOI_{SD}^2)^2}$$

$$\frac{\partial RVS}{\partial AOI}=\frac{a_1+2a_2AOI}{(a_0+a_1AOI_{SD}+a_2AOI_{SD}^2)}$$

Table 1: Data used in FP-10 part 1 analysis. Angles correspond to middle of sample range (referenced to M1).

UAID	Collects	SIS Scan Angle	SIS HAM AOI	Samples Used	Collect Window
4303155	1-3	-66.31	60.73	0-47	SV
4303156	1-3	-9.11	38.89	522-569	2
4303157	1-3	-39.38	49.81	948-995	0
4303158	1-3	4.58	34.79	1292-1339	2
4303159	1-3	-46.18	52.49	566-613	0
4303160	1-3	-9.20	38.92	517-564	2
4303161	1-3	-56.24	56.56	0-47	0
4303162	1-3	20.87	31.02	1144-1191	3
4303163	1-3	-31.11	46.64	1413-1460	0
4303164	1-3	-9.20	38.92	517-564	2
4303165	1-3	-52.37	54.98	218-265	0
4303166	1-3	36.84	28.93	978-1025	4
4303168	1-3	-21.44	43.09	893-940	1
4303169	1-3	53.72	28.84	1927-1974	4
4303170	1-3	-9.17	38.91	519-566	2

Table 2: Data used in FP-10 part 2 analysis. Angles correspond to middle of sample range.

UAID	Collect	LABB Scan Angle	LABB HAM AOI	Samples Used	Collect Window
4302125	1	-8.87	38.81	1321-1370	2
4302126	1	-66.42	60.77	213-262	0
4302127	1	21.31	30.94	890-939	4
4302128	1	-45.88	52.37	1368-1417	0
4302129	1	5.21	34.62	1049-1098	3
4302130	1	-8.87	38.81	1321-1370	2
4302131	1	-56.27	56.57	784-833	0
4302132	1	-20.81	42.86	650-699	2
4302133	1	-38.79	49.58	703-752	1
4302134	1	-8.87	38.81	1321-1370	2
4302135	1	-51.73	54.72	1039-1088	0
4302136	1	34.38	29.14	1625-1674	4
4302137	1	-30.76	46.51	1154-1203	1
4302138	1	-8.87	38.81	1321-1370	2
4302139	1	-61.32	58.65	500-549	0

Table 3: Comparison of reflective band average RVS uncertainties.

Band	Uncertainty [2]	Uncertainty
I1	0.026	0.067
I2	0.019	0.032
I3	0.018	0.046
M1	0.036	0.096
M2	0.025	0.080
M3	0.021	0.074
M4	0.020	0.069
M5	0.015	0.085
M6	0.017	0.111
M7	0.013	0.059
M8	0.021	0.019
M9	0.197	0.026
M10	0.011	0.021
M11	0.017	0.028

Table 4: Comparison of thermal band average RVS uncertainties.

Band	Uncertainty [1]	Uncertainty
I4	0.035	0.137
I5	0.080	0.134
M12	0.034	0.062
M13	0.041	0.059
M14	0.093	0.059
M15	0.072	0.048
M16A	0.054	0.057
M16B	0.056	0.057

Figure 1: Final RVS uncertainty per reflective band (detector 9, HAM side A) versus HAM AOI.

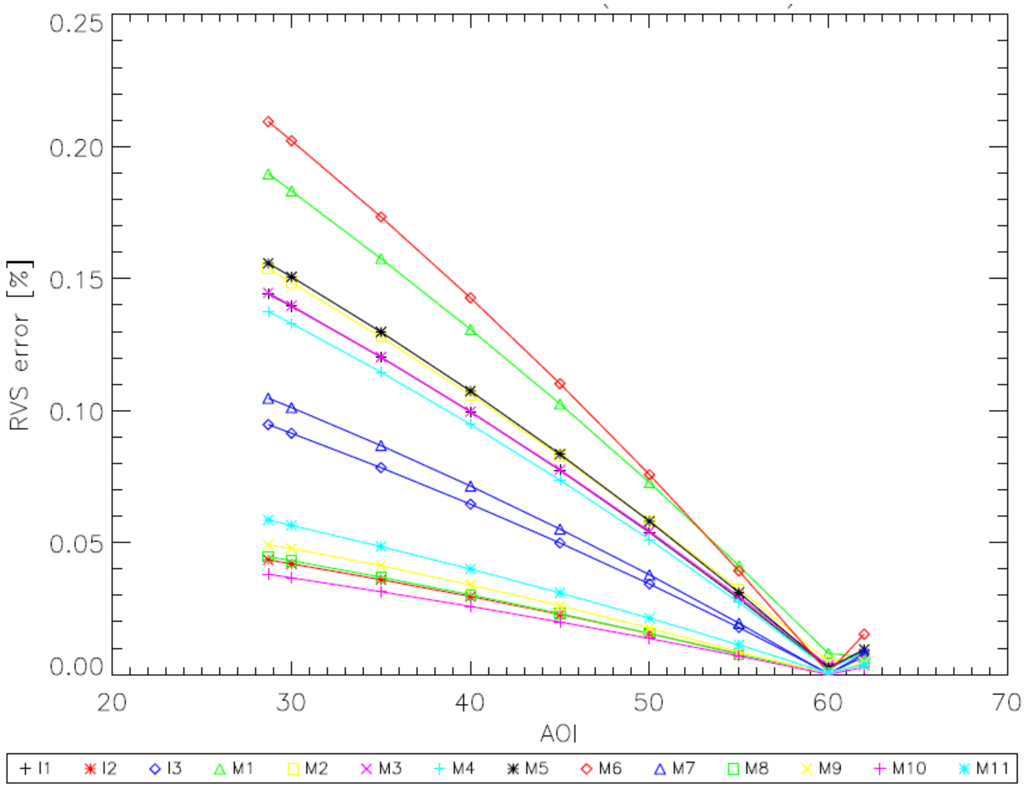

Figure 2: Band I1 RVS (detector 9, HAM side A) with uncertainty versus HAM AOI.

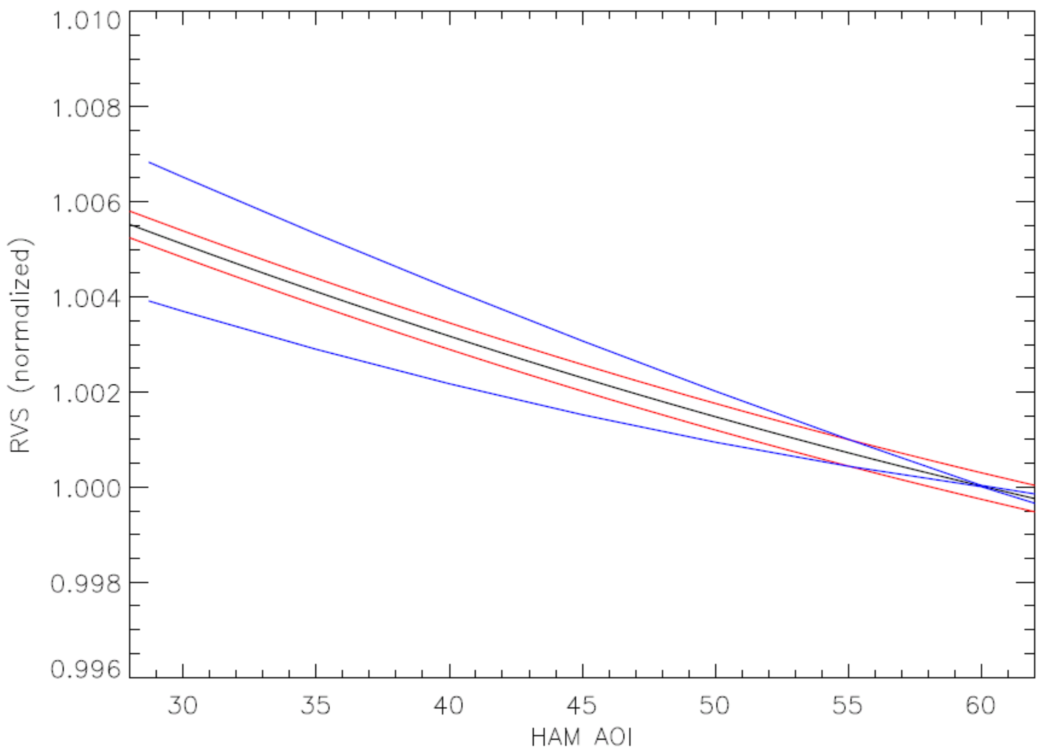

Figure 3: Band I2 RVS (detector 9, HAM side A) with uncertainty versus HAM AOI.

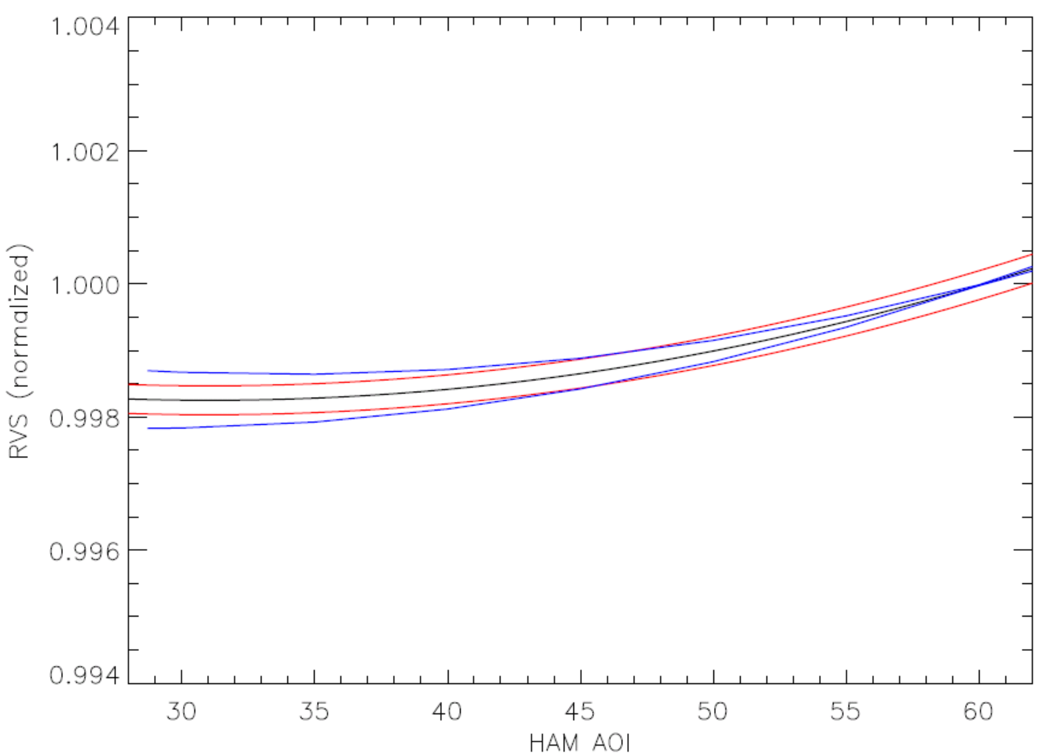

Figure 4: Band I3 RVS (detector 9, HAM side A) with uncertainty versus HAM AOI.

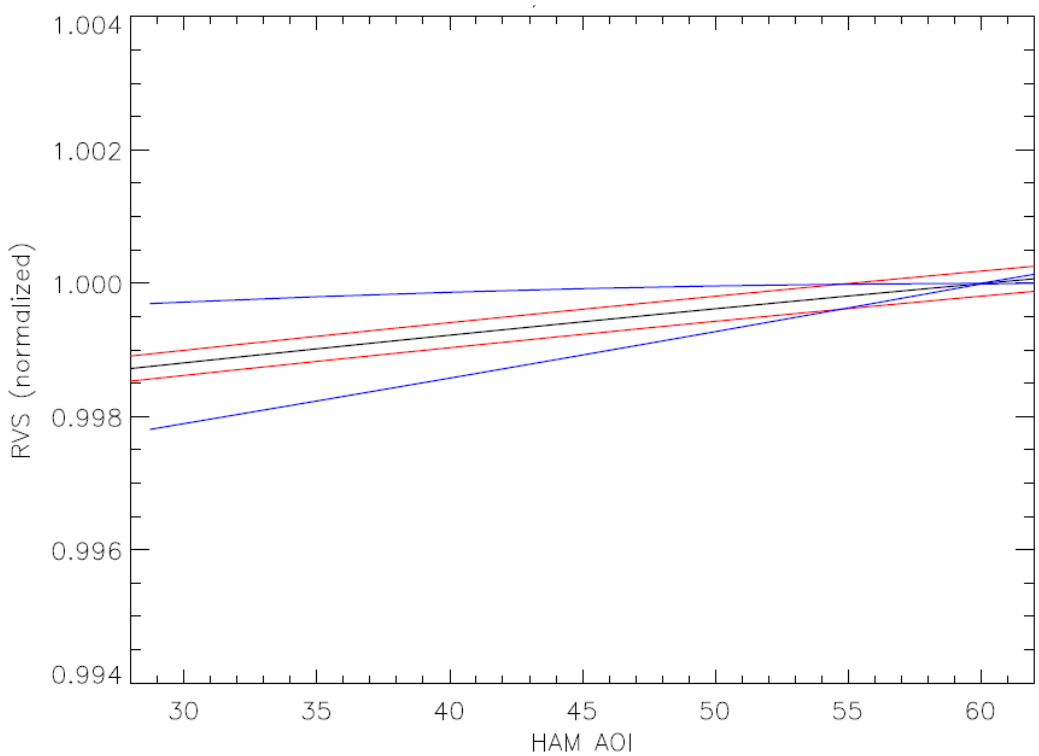

Figure 5: Band M1 RVS (detector 9, HAM side A) with uncertainty versus HAM AOI.

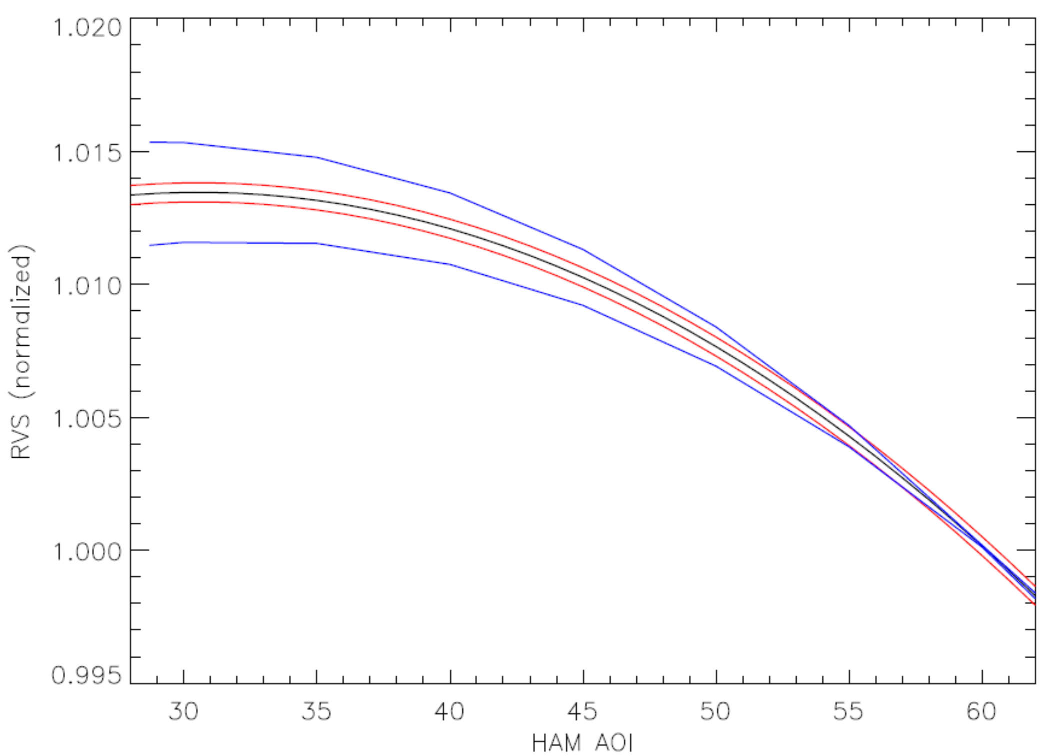

Figure 6: Band M2 RVS (detector 9, HAM side A) with uncertainty versus HAM AOI.

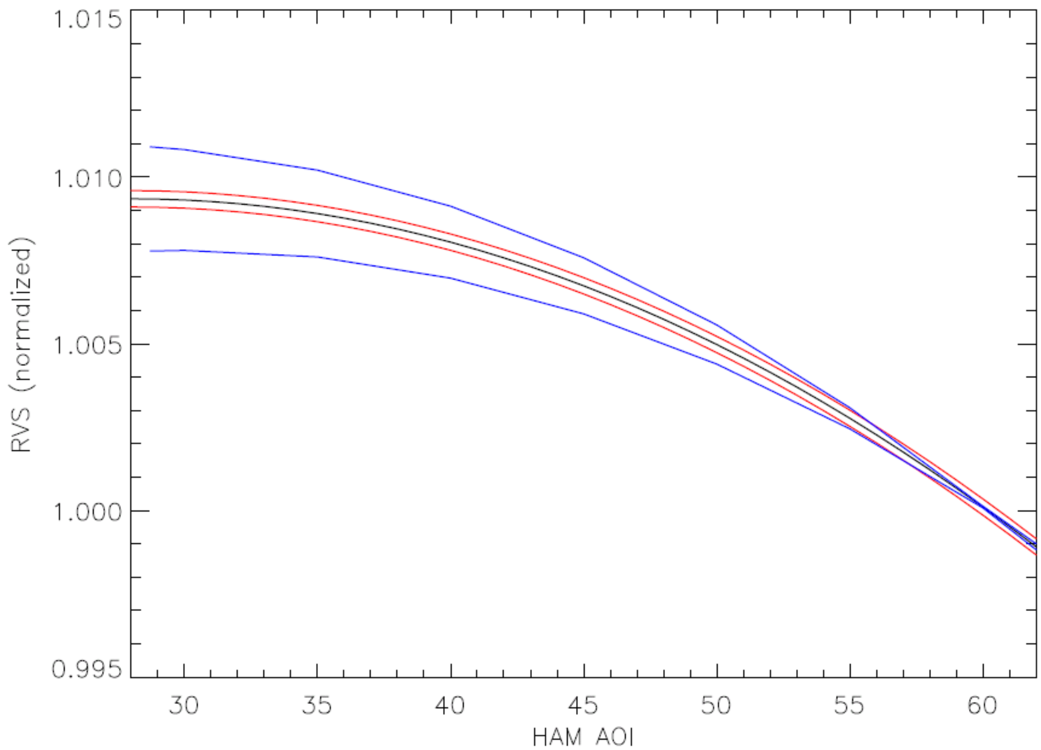

Figure 7: Band M3 RVS (detector 9, HAM side A) with uncertainty versus HAM AOI.

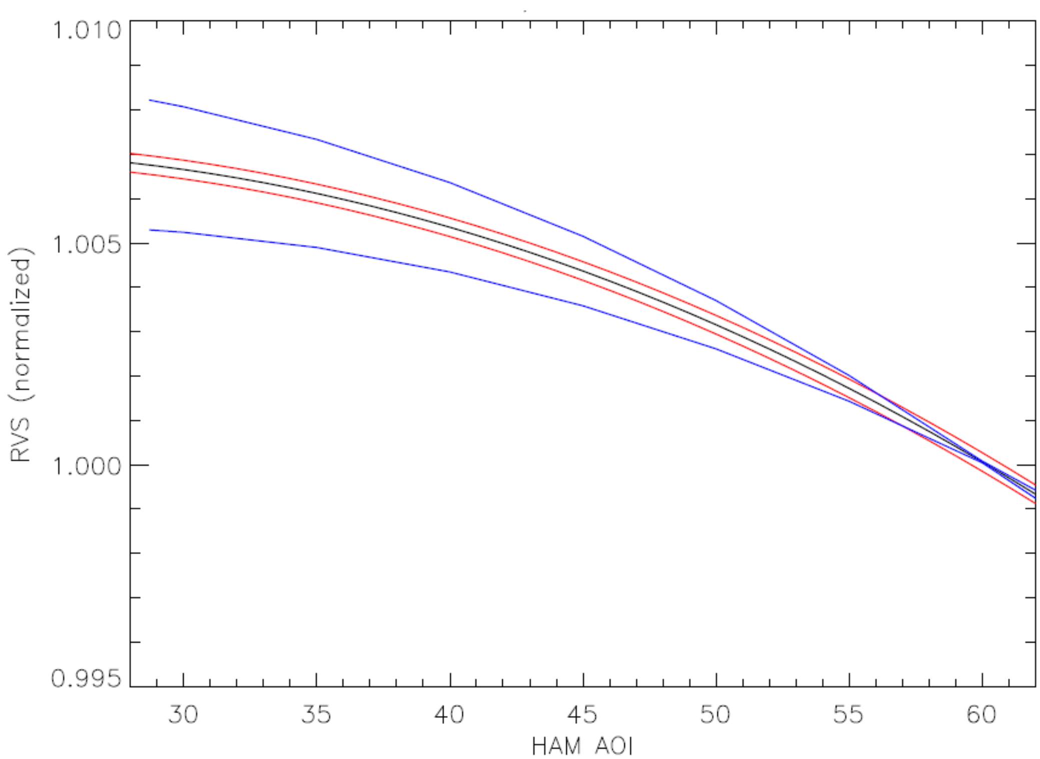

Figure 8: Band M4 RVS (detector 9, HAM side A) with uncertainty versus HAM AOI.

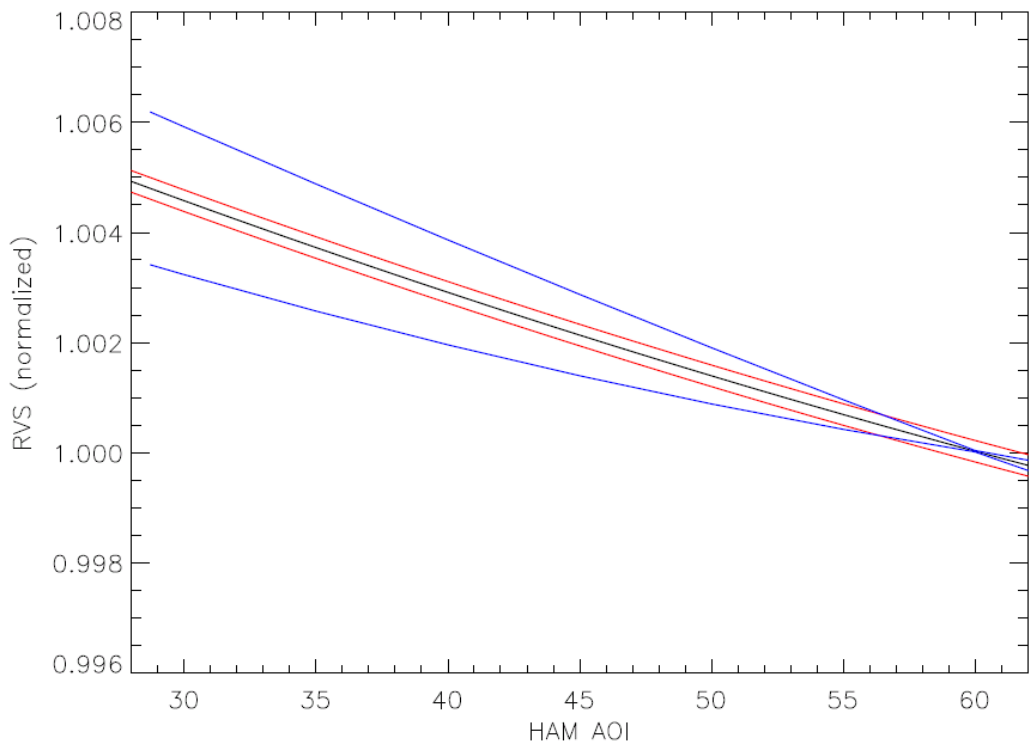

Figure 9: Band M5 RVS (detector 9, HAM side A) with uncertainty versus HAM AOI.

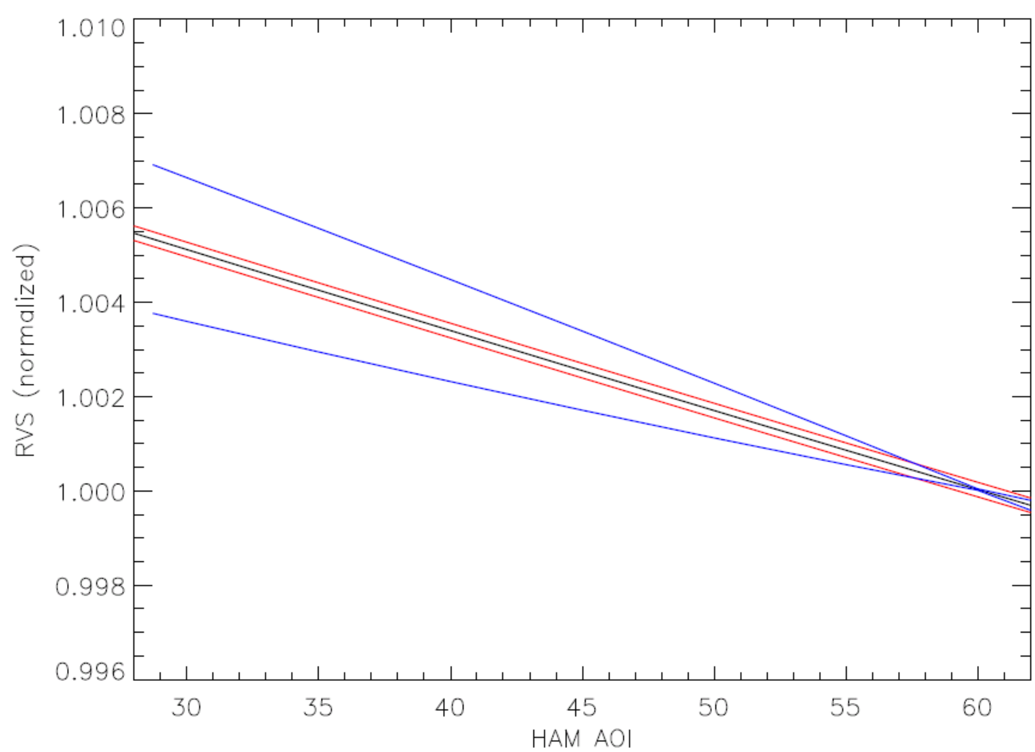

Figure 10: Band M6 RVS (detector 9, HAM side A) with uncertainty versus HAM AOI.

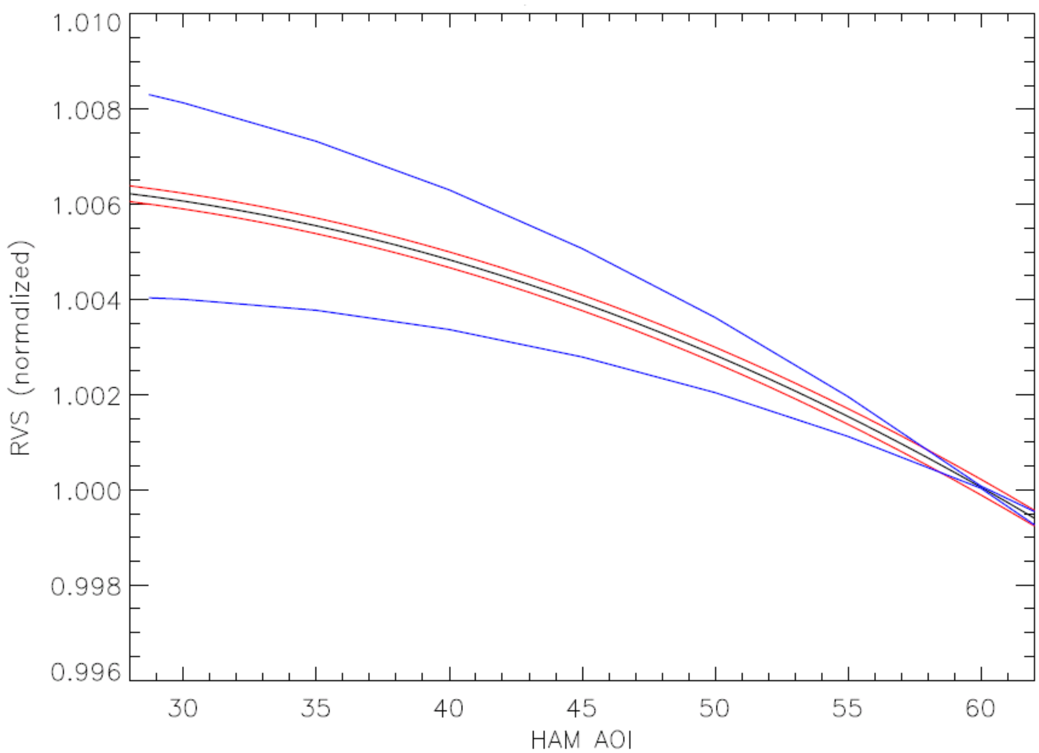

Figure 11: Band M7 RVS (detector 9, HAM side A) with uncertainty versus HAM AOI.

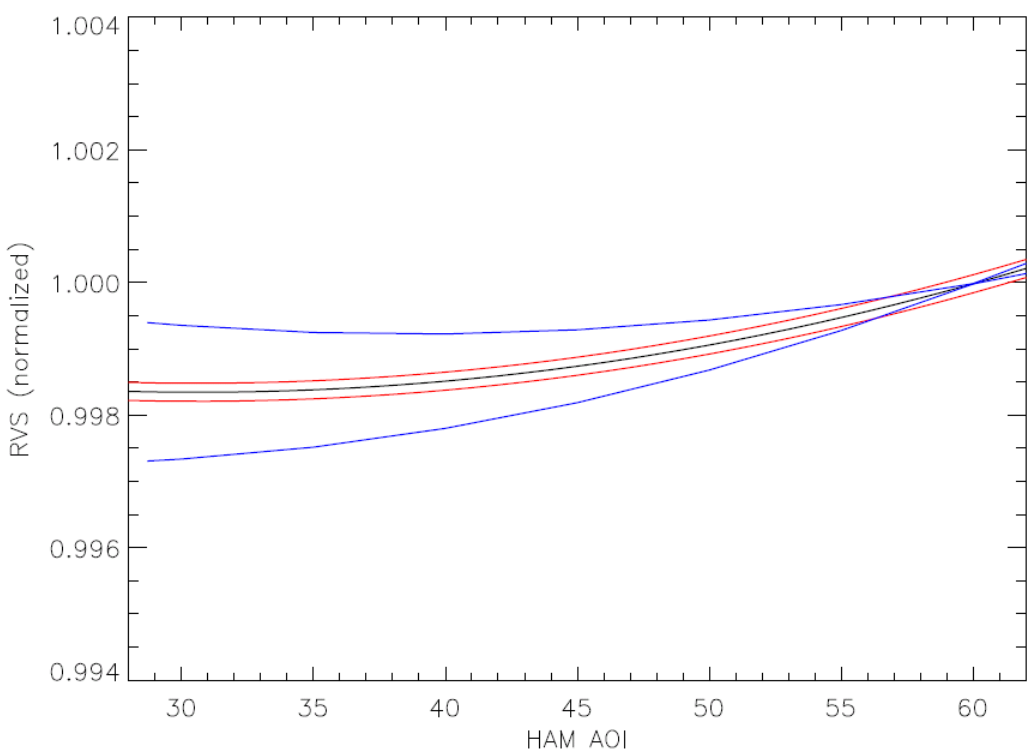

Figure 12: Band M8 RVS (detector 9, HAM side A) with uncertainty versus HAM AOI.

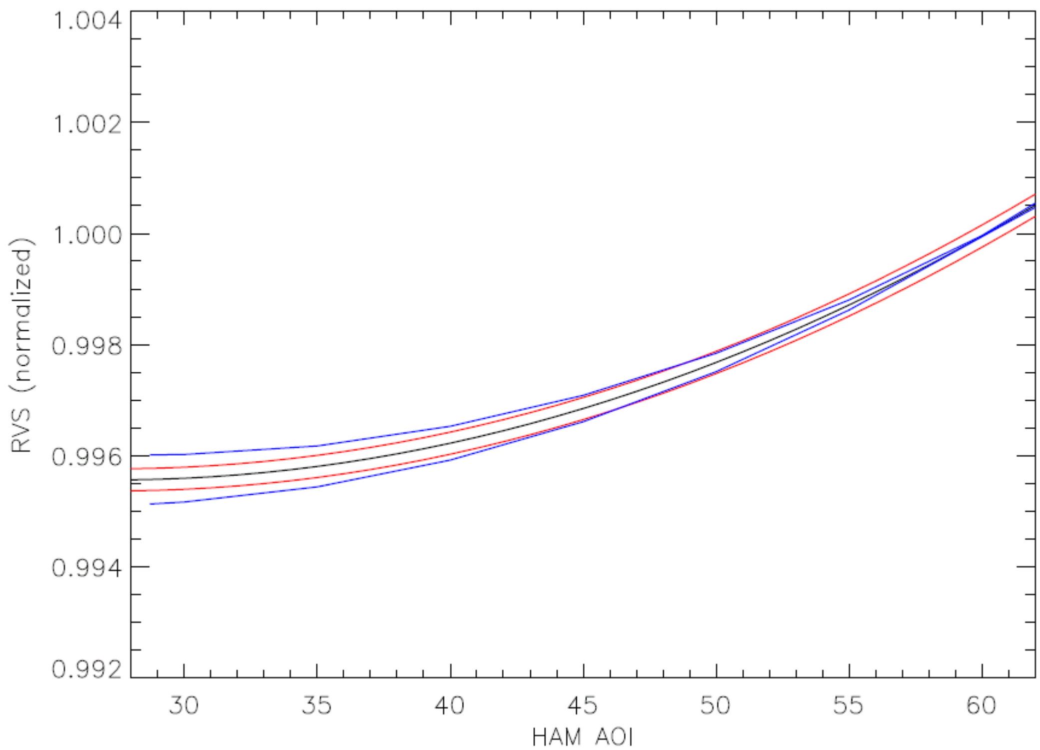

Figure 13: Band M9 RVS (detector 9, HAM side A) with uncertainty versus HAM AOI.

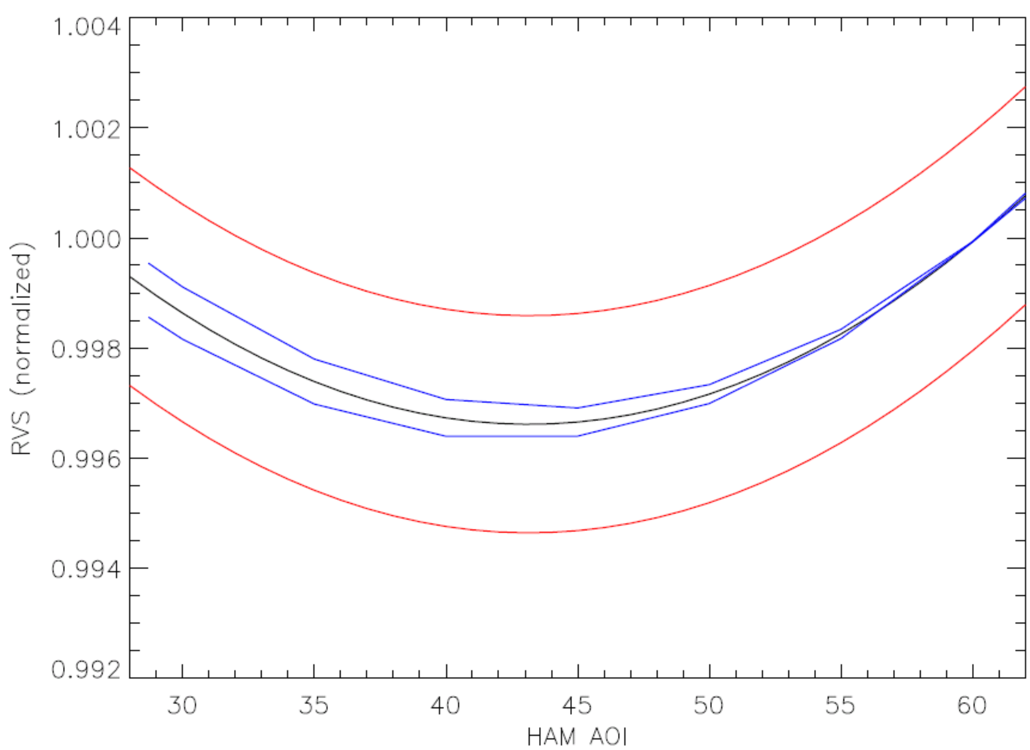

Figure 14: Band M10 RVS (detector 9, HAM side A) with uncertainty versus HAM AOI.

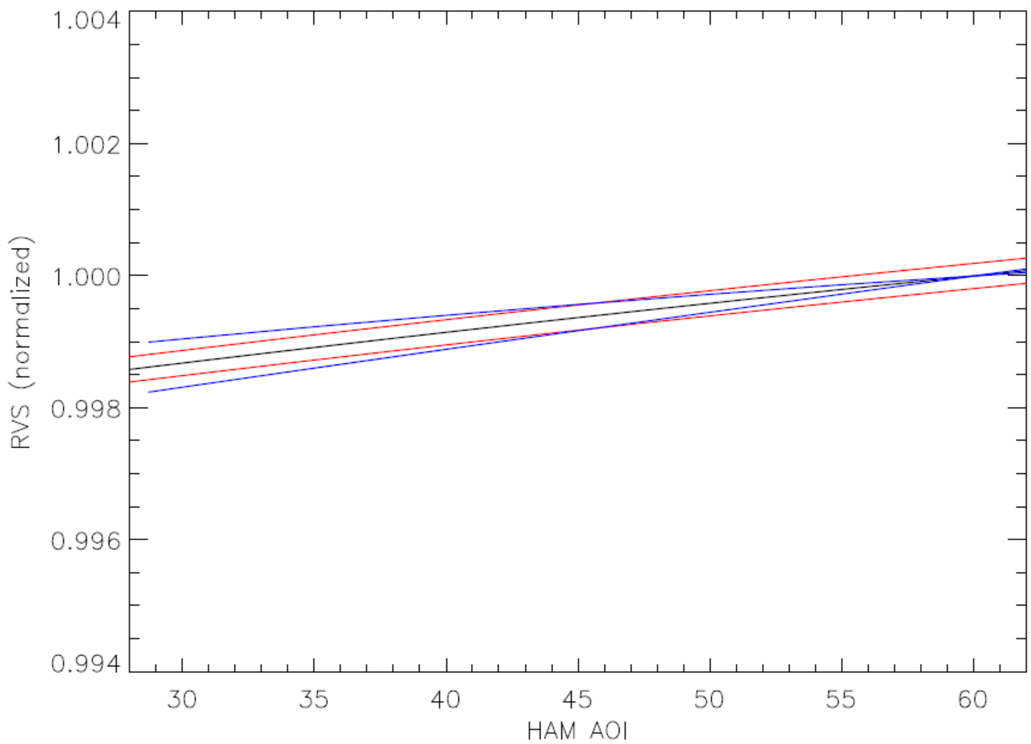

Figure 15: Band M11 RVS (detector 9, HAM side A) with uncertainty versus HAM AOI.

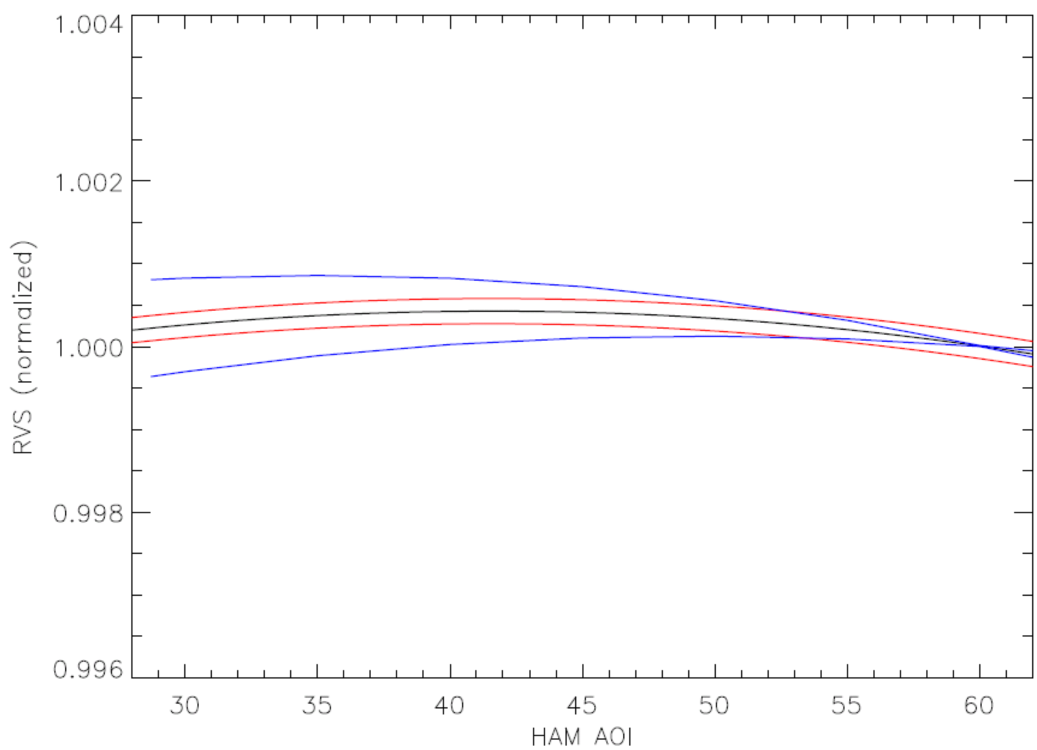

Figure 16: Final RVS uncertainty per thermal band (detector 9, HAM side A) versus HAM AOI.

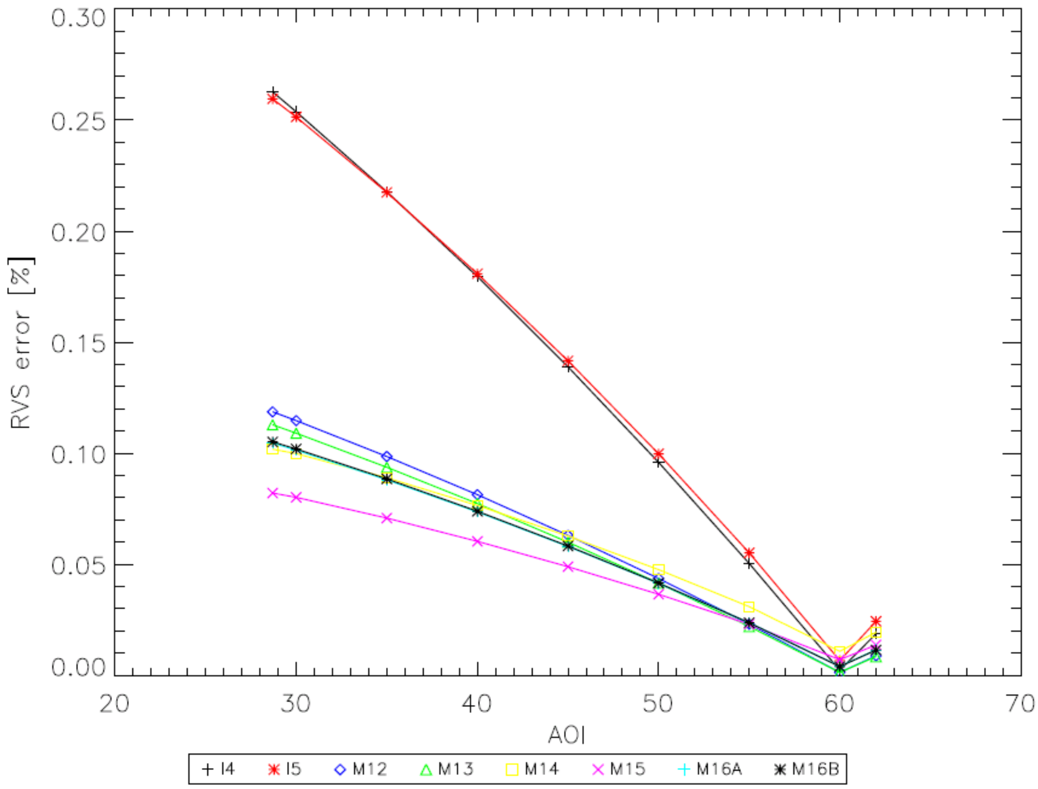

Figure 17: Band I4 RVS (detector 9, HAM side A) with uncertainty versus HAM AOI.

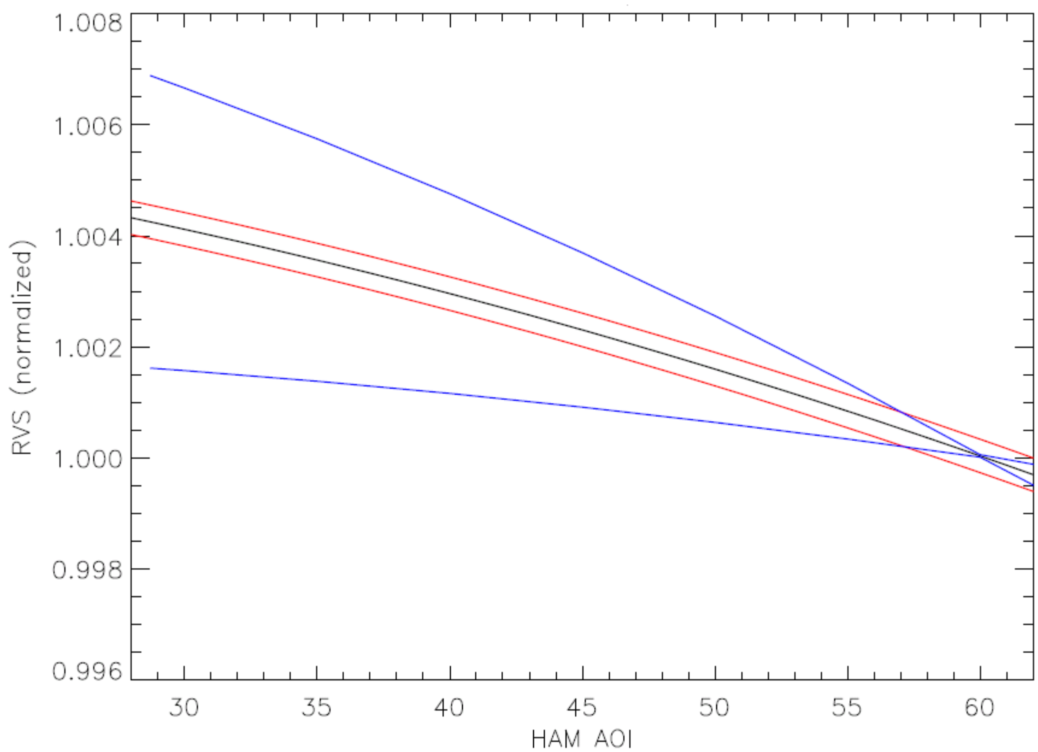

Figure 18: Band I5 RVS (detector 9, HAM side A) with uncertainty versus HAM AOI.

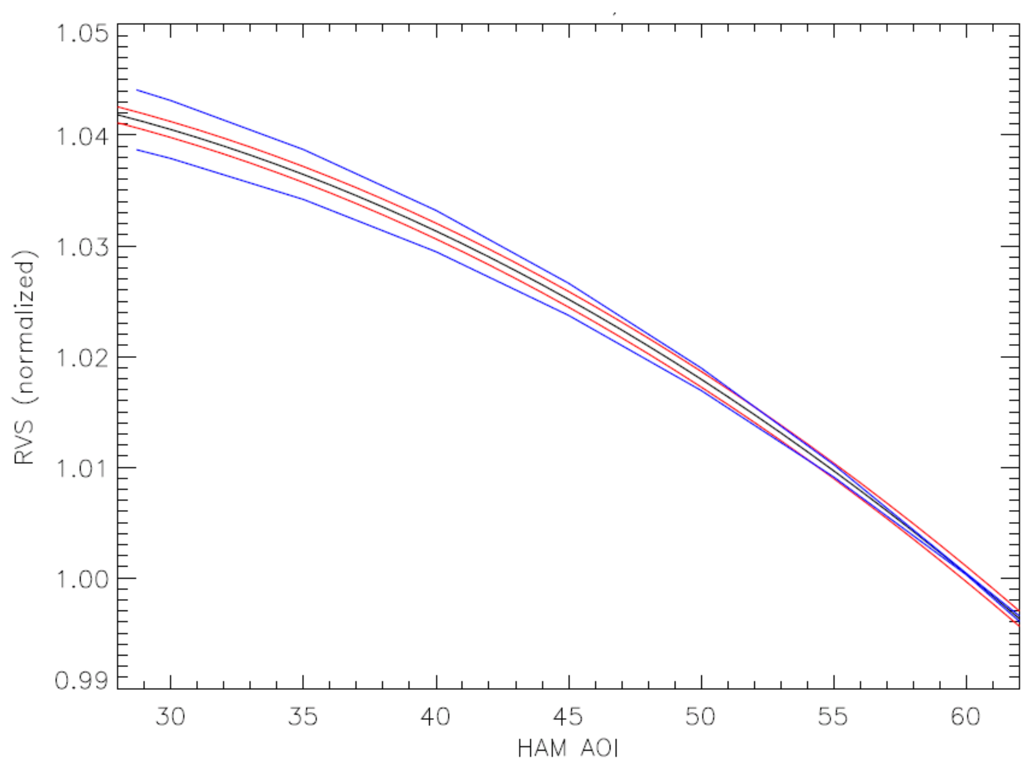

Figure 19: Band M12 RVS (detector 9, HAM side A) with uncertainty versus HAM AOI.

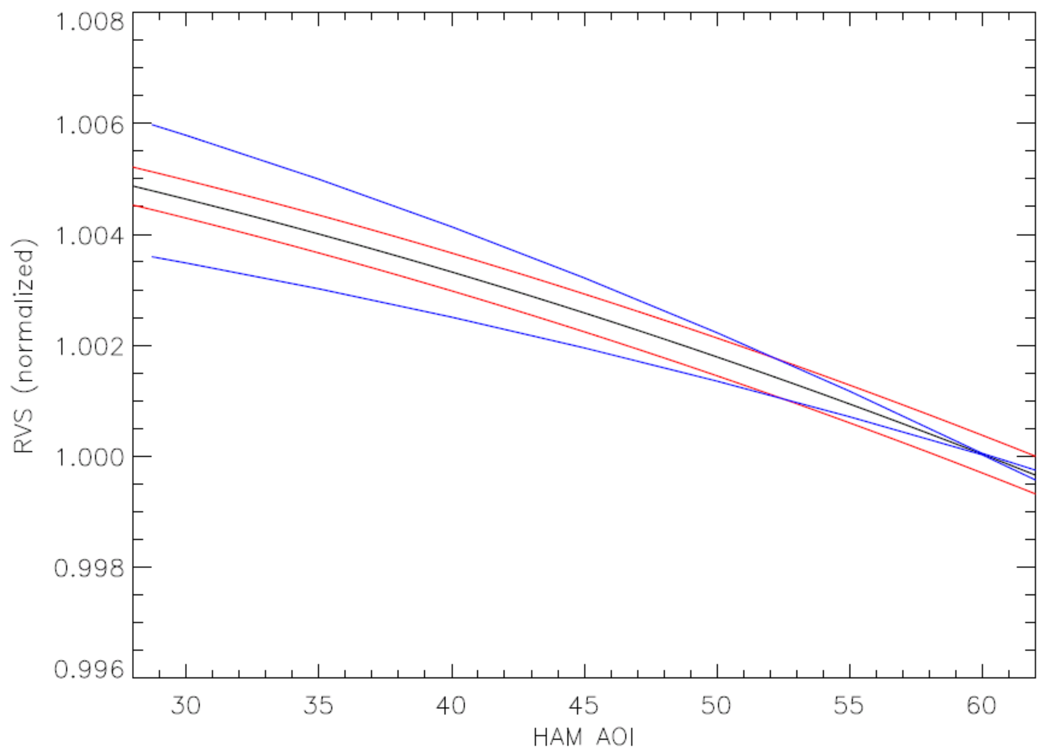

Figure 20: Band M13 RVS (detector 9, HAM side A) with uncertainty versus HAM AOI.

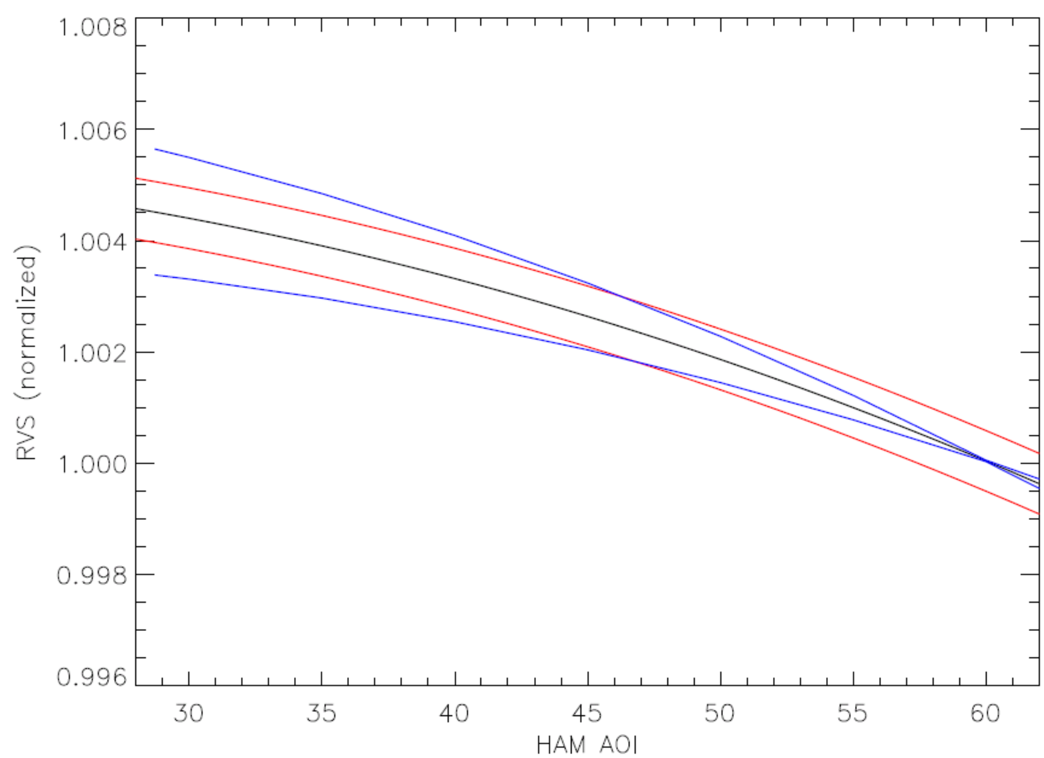

Figure 21: Band M14 RVS (detector 9, HAM side A) with uncertainty versus HAM AOI.

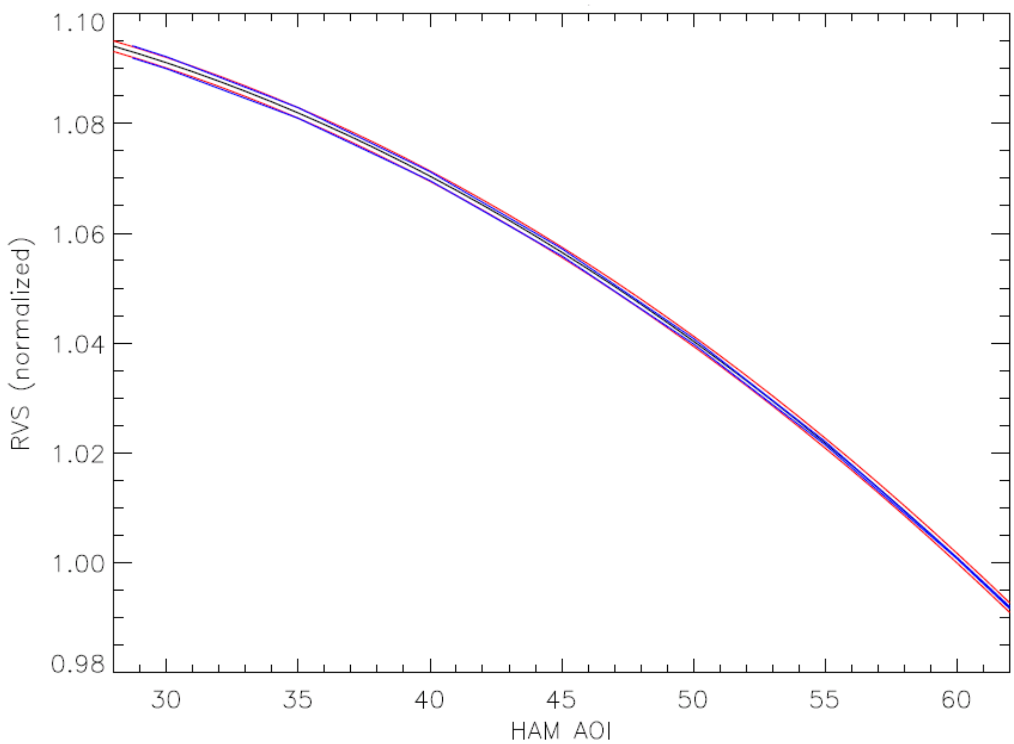

Figure 22: Band M15 RVS (detector 9, HAM side A) with uncertainty versus HAM AOI.

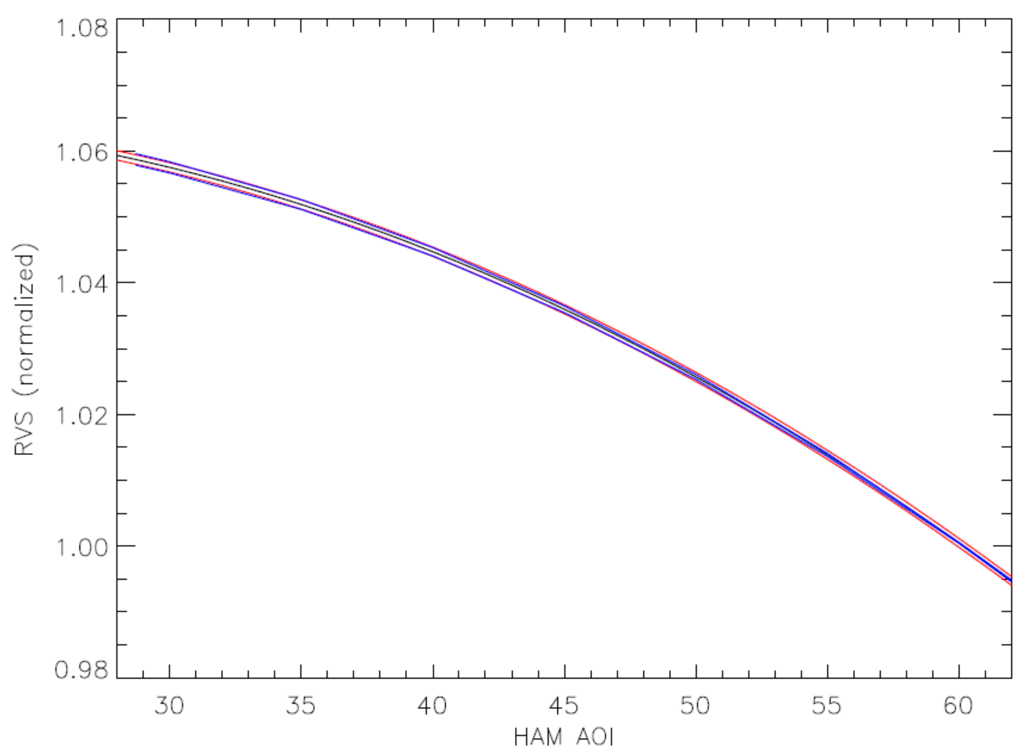

Figure 23: Band M16A RVS (detector 9, HAM side A) with uncertainty versus HAM AOI.

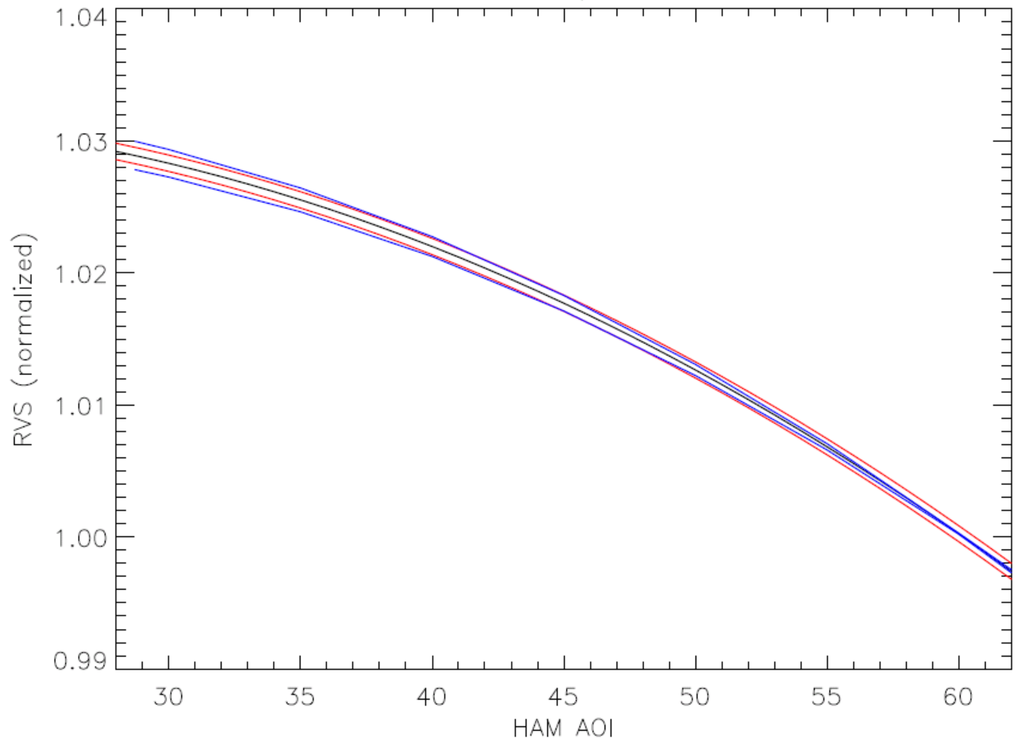

Figure 24: Band M16B RVS (detector 9, HAM side A) with uncertainty versus HAM AOI.